Nonlinear interferometric vibrational imaging: Optical ranging and spatial localization of CARS

Stephen A. Boppart[*a-d], Daniel L. Marks[a,b], Jeremy S. Bredfeldt[a,b], Claudio Vinegoni[a,b]

[a]Department of Electrical and Computer Engineering,
[b]Beckman Institute for Advanced Science and Technology,
[c]Department of Bioengineering,
[d]College of Medicine
University of Illinois at Urbana—Champaign, Urbana, IL USA 61801

ABSTRACT

Diagnostic imaging trends are progressing toward the molecular level with the advent of molecular imaging techniques. Optical molecular imaging techniques that utilize targeted exogenous contrast agents or detect endogenous molecular signatures will significantly extend our ability to detect early pathological changes in biological tissue, and treat diseases early when they are most amenable to be cured. We have developed a technique called Nonlinear Interferometric Vibrational Imaging (NIVI) that takes advantage of the coherent nature of coherent anti-Stokes Raman scattering (CARS) processes and the coherent optical ranging and imaging capabilities of optical coherence tomography (OCT). OCT uses interferometry and heterodyne detection in the time or spectral domain to localize reflections of near-infrared light deep from within highly-scattering tissues. OCT has found wide biological and medical applications, and recently, molecular imaging methods have been developed. By utilizing the molecular-sensitivity of CARS, NIVI performs optical ranging and multi-dimensional molecular imaging with OCT-like optical systems, enabling the retrieval of not only $\chi^{(3)}$ [chi$^{(3)}$] amplitude but also phase information, the rejection of problematic non-resonant background four-wave-mixing signals, enhanced sensitivity from heterodyne detection, and a relaxation of the high-numerical aperture focusing requirements present in CARS microscopy. We present recent progress and advances in NIVI, including depth-ranging capabilities that extend significantly deeper than current CARS microscopy methods and are potentially more suitable for cross-sectional deep-tissue *in vivo* imaging.

Keywords: Coherent Anti-Stokes Raman Scattering, Optical Coherence Tomography, spectroscopy, nonlinear optics

1. INTRODUCTION

There are many clinical situations in which non-invasive, high-resolution imaging could be useful for locating and diagnosing pathological tissue as an alternative or an additional procedure to traditional histopathology. Optical coherence tomography (OCT) has proved to be a successful modality for imaging at the 2-20 μm length scales[1-4]. However, it is limited in applicability by the properties is measures, that is the linear scattering properties of specimens. These linear properties can indicate the absorption[5-7], refractive index[8,9], scattering, and birefringence[10-13] of a specimen, but do not encode the density of specific molecules. Unfortunately, these linear properties can be quite similar in different tissues, limiting the ability of OCT to distinguish between tissue types, such as pathological versus normal. To address this problem, two new OCT techniques are being studied that use molecular differences to provide more useful OCT contrast. The first technique uses exogenous contrast agents that can be targeted to bind to specific molecules to obtain molecular specificity[14,15]. The second technique, which was recently proposed[16] and demonstrated[17], exploits coherent, nonlinear optical methods to identify endogenous molecular properties. One example, a method called Second Harmonic OCT (SH-OCT), was used to image biological tissue[18]. Although SH-OCT can differentiate between certain classes of tissues, for example collagen versus adipose tissue, unambiguous molecular identification cannot be achieved.

[*] Inquiries should be directed to *boppart@uiuc.edu*, Telephone: 1-217-244-7479

Multiphoton Microscopy in the Biomedical Sciences V, edited by Ammasi Periasamy, Peter T. C. So, Proceedings of SPIE Vol. 5700 (SPIE, Bellingham, WA, 2005)
1605-7422/05/$15 · doi: 10.1117/12.592862

Instead, we use a well-known optical molecular identification tool called Coherent Anti-Stokes Raman Scattering (CARS).

In this paper, we present a demonstration of a CARS-sensitive tomographic optical ranging technique for mapping the presence of a specific molecule within a sample. CARS is a vibrational spectroscopy technique that has found wide application in condensed matter physics, chemistry, and more recently in nonlinear microscopy[19]. It relies on a stimulated interaction between the incident photons and the Raman-active phonons in a sample. When this interaction occurs, the incident photon may be shifted in energy, either up or down, by the Raman-active phonon energy present in the sample. Since the vibrational characteristics of molecular bonds are quite specific, a CARS spectrum can be measured that often allows for the molecule to be identified. The resulting molecular selectivity of CARS has motivated its use as a molecular contrast mechanism for microscopy that alleviates the need for staining with fluorescent dyes to generate contrast as in confocal microscopy.

In CARS spectroscopy, the frequencies of two incident laser pulses, ω_p (pump) and ω_s (Stokes), are chosen such that the difference frequency $\omega_v=\omega_p-\omega_s$ is equal to a Raman-active vibrational mode of the molecule under study. When the pump and Stokes photons are focused to the same point in the sample, and a molecule with the proper vibrational properties is present within the focal volume, a CARS photon is generated. This CARS photon results from a four-wave-mixing process and is generated in the phase-matching direction at the complementary anti-Stokes frequency $\omega_{AS}=2\omega_p-\omega_s$. To obtain a CARS spectrum for the sample, the Stokes frequency is swept to probe for the presence of other Raman-active modes, and the emitted anti-Stokes intensity is measured as a function of ω_v.

In addition to its molecular identification capabilities, CARS is also emitted coherently with respect to the incident photons, and due to this coherent nature, it can be measured interferometrically[20]. Our technique takes advantage of this property to provide molecular contrast for interferometric optical ranging where the axial resolution is defined by the coherence length of the CARS pulse. CARS microscopy[19,21-27] scans a tightly focused beam through tissue to produce a nonlinear Raman effect in a confined region. Incoherently detected CARS is unable to distinguish between photons emitted at various points inside the focal region, so the focal region must be small to achieve high resolution. Therefore to scan a large volume requires serially scanning many small focal volumes and a relatively long scanning time.

In conventional OCT, microstructural features in tissue are distinguished within the focal volume by the time of arrival of the signal using interferometric detection. When a low numerical aperture objective is used, a large diameter beam is created with a larger depth-of-field. This enables OCT to scan a larger volume at a lower resolution, with the time of arrival used rather than a tight focus to distinguish depth. Because the anti-Stokes radiation in CARS is emitted coherently with respect to the pump and Stokes radiation, it too can be distinguished interferometrically by its time of arrival, enabling this scanning mode to be used. Similar to OCT then, time-of-flight information can be used to locate the position of a molecule along the depth-of-field of the focusing objective. Furthermore, a three-dimensional map of the specified molecule within the sample can be generated by taking multiple axial scans at different lateral positions.

A schematic of this interferometric CARS ranging system is shown in Figure 1. An illumination source consisting of a laser pulse, or a pair of laser pulses, is used as the pump and Stokes radiation and will be used to generate CARS. The illumination can be shaped to stimulate a particular Raman resonance frequency of a target molecular species. The illumination is then split in two by a beam splitter to perform interferometry. The illumination in the sample arm of the interferometer is focused into the specimen by a low numerical aperture objective. The incident illumination will either be scanned or the specimen will be translated laterally to acquire adjacent axial depth scans. The transverse resolution is dependent on the beam width through the specimen, and the axial resolution is given by the arrival time of the anti-Stokes. The backscattered anti-Stokes is collected from the specimen and separated from the pump and Stokes beams by a dichroic beamsplitter. In the reference arm of the interferometer, the illumination is focused into a sample with the same resonance frequency as the target species. The forward-scattered light is collected and interferometrically cross-correlated with the light form the specimen. This cross-correlation can be performed in either the time domain or the frequency domain. The peaks of the cross-correlation will correspond to the anti-Stokes scatterers in the sample, and the interference fringes generated can be used to extract phase information.

In this technique, backscattered CARS is detected. However, phase matching favors forward-scattering CARS in bulk materials. Backscattering can occur if the target species is present as randomly positioned subwavelength-sized particles. In this case, the phase matching condition of a bulk medium is relaxed and the CARS is emitted directly into the backscattered direction, producing epi-CARS[28]. A second means for backscattering of CARS to occur is if forward emitted CARS is subsequently linearly backscattered by another small particle within the focal volume, or from other scattering particles or interfaces within the incident beam path. However, since a particle close to the Raman scatterer is

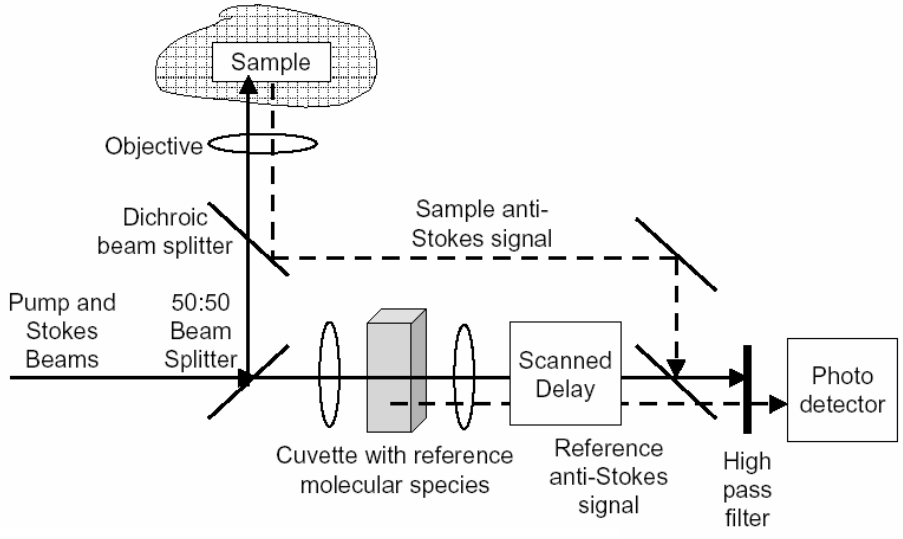

Figure 1: Schematic of interferometric CARS ranging.

more likely to backscatter the anti-Stokes light than a more distant particle, we expect that the spatial localization of the imaging will be preserved. It is likely that both of these mechanisms contribute to the detected backscattered CARS.

A significant advantage of using low numerical aperture focusing is that an entire axial scan can be taken at once, analogous to Spectral Domain Optical Coherence Tomography (SD-OCT)[29,30]. By using spectral detection, the backscattered radiation generated by a single illumination pulse can be measured instantaneously. This can significantly increase data acquisition rates because only one pulse need be used for each axial scan, in contrast to CARS microscopy which scans one point at a time. Therefore far fewer pulses are needed when a lower numerical aperture objective is used. By using fewer pulses, the individual pulse energy can be made greater while keeping average power low. This can help boost the instantaneous intensity to make up for the larger focal spot size. If a 1-kHz repetition rate millijoule regenerative amplifier is used as the illumination source, 1000 axial scans can be taken per second, with each pulse being of microjoule energy, but maintaining only milliwatts of average power on the tissue.

The axial resolution of this method will depend, like standard OCT, on the bandwidth of the returned signal from the sample. It is desirable to maximize the bandwidth of the anti-Stokes light emitted to achieve the best range resolution. At the same time, we would like to only stimulate a single Raman resonance specific to a particular molecular species. This can be achieved by utilizing various broadband CARS excitation schemes, such as utilizing a pair of overlapped chirped pulses[31,32], or applying a periodic perturbation to the pulse in the spectral domain[33-36]. Because these pulses are broadband the anti-Stokes radiation will also be broadband, but the envelope of the pulse is shaped to only stimulate a particular Raman feature. These methods enable the pulse to be stretched out to minimize peak power but can excite a large Raman polarization. Another possibility is to use a pump/Stokes/probe combination where the pump and Stokes are narrowband to stimulate the Raman resonance, but the probe pulse is broadband to create a broad anti-Stokes spectrum. However, this presents the problem of obtaining synchronized broadband and narrowband pulses.

2. COHERENT INTERFEROMETRIC RANGING OF CARS

Our approach presented here is somewhat different than the method outlined above in that it generates the reference pulse in an alternate way. Because this is a heterodyne method, a reference pulse must be generated with a frequency identical to the CARS returning from the sample. This may be achieved in other ways than using an identical sample in the reference arm. To generate a Stokes pulse, we used a second-harmonic optical parametric oscillator (SHG-OPA), which converts the second-harmonic of the pump pulse to signal and idler pulses. This process is illustrated in Figure 2. The SHG-OPA consists of two three-wave-mixing processes that is equivalent to a single four-wave-mixing process. The SHG-OPA is used to generate an idler pulse that acts as the Stokes pulse that in combination with the pump pulse stimulates CARS in the sample. At the same time, the signal pulse generated by the SHG-OPA is the same frequency as the anti-Stokes created by the sample. Therefore, the signal from the SHG-OPA can be used as a reference pulse to demodulate the anti-Stokes signal. Use of the SHG-OPA is a convenient means to create a Stokes pulse and a reference

pulse at the same time that are automatically matched, since the SHG-OPA and CARS are both four-wave-mixing processes.

We now describe, in detail, the experimental setup shown in Figure 3. Ten percent of the output of a femtosecond, microjoule chirped-pulse amplification system (RegA 9000, Coherent Inc) is used as the pump pulse, while the rest is used to pump the SHG-OPA (OPA 9450, Coherent Inc.). The output of the OPA consists of two pulses, the Stokes and the anti-Stokes, each separated in energy from the pump by an equal amount. These input pulses represent the sources for our interferometer. The reference arm pulse is created by separating the anti-Stokes pulse from the OPA output using a dichroic beamsplitter, sending this reference pulse through a variable optical delay line, and coupling it into a 3dB single mode fiber coupler. We then use an attenuated pump pulse from the amplifier and the Stokes pulse from the OPA, centered at 1047 nm, as the incident sample arm pulses. These are collinearly and temporally overlapped at another dichroic beamsplitter and then focused into the sample using a 30 mm focal length achromatic lens. With a total incident power on the sample of 1.5 mW, anti-Stokes photons are generated at locations where the appropriate molecule is present. The backscattered photons are then separated out with a third dichroic beamsplitter and coupled into the single mode fiber coupler. As the reference arm pathlength is scanned, the output of the fiber coupler is monitored with an avalanche photodiode operating in photon counting mode. Finally, interference is measured and plotted as a function of delay position.

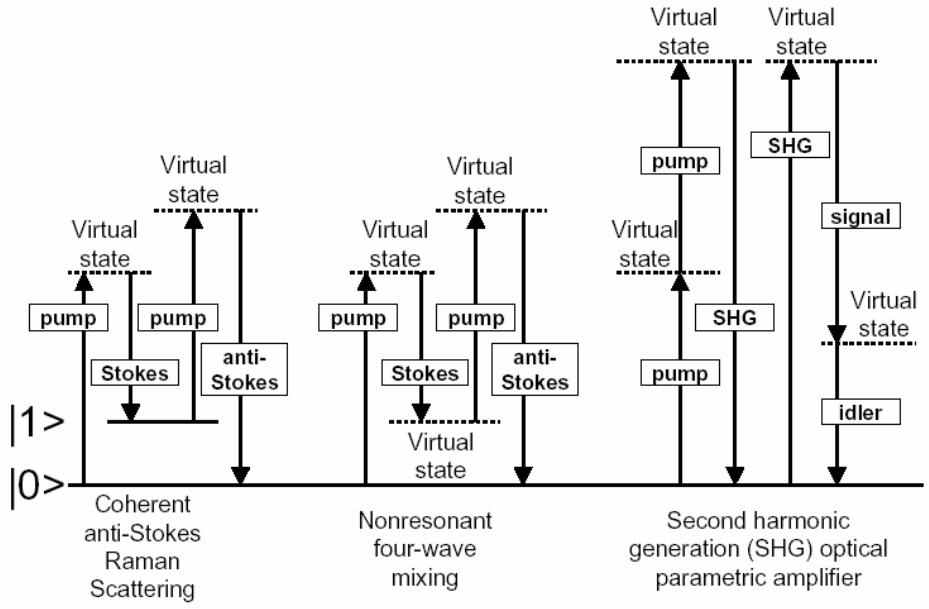

Figure 2: Diagram of four-wave-mixing processes utilized in CARS (left), nonresonant four-wave-mixing (middle), and the four-wave-mixing process mediated by two three-wave-mixing processes in a second-harmonic-generation optical parametric amplifier (right).

The molecular species we use in our sample is acetone which has a Raman-active vibrational mode at 2952 cm^{-1} associated with the C-H stretch vibration. The resulting CARS pulse is centered at 647 nm. The autocorrelation of this pulse was previously characterized and the measured signal was shown to result from a four-wave-mixing process since

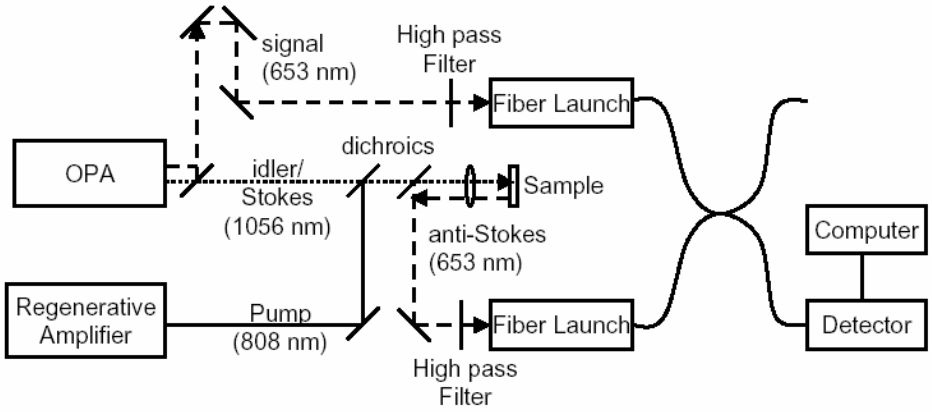

Figure 3: Experimental set-up to measure CARS interferograms for coherent ranging.

it was linearly related to the Stokes intensity and quadratically related to the pump intensity[17]. Moreover, this process is CARS resonance because, when the Stokes wavelength is tuned to the Raman-active vibrational mode in acetone, the anti-Stokes power is maximized.

The sample structure we use to demonstrate coherent ranging of CARS[37] is shown in Figure 4. It is constructed by sandwiching two 100 μm-thick wells of acetone between 150 μm-thick coverslips. The thickness of each layer in the drawing represents the optical path length through the sample. An air-filled well, lined by two cover slips, is placed in between the two wells of acetone physically separating them by approximately 600 μm. It is important to note here that this air gap is necessary to show that the signal measured from the second well of acetone is not simply backscattered CARS generated in the first well, but, in fact, CARS generated from the second well. To prove that CARS is generated and backscattered from both wells of acetone, we place the sample such that the second layer of acetone is at the focus, and therefore, the measured interference from this layer is greater in amplitude than that from the first.

Figure 4(a,b) shows the demodulated interferometric axial measurement of the sample using normal OCT and NIVI. Standard optical ranging (Figure 4(a)) is not molecularly sensitive, therefore it produces a reflection at each of the interfaces present in the sample. The molecular contrast ranging measurement (Figure 4(b)) contains only two peaks corresponding to the two separate acetone layers present in the sample. Since the interference results from scattering at the second acetone-glass interface in each well, these peaks represent the point spread function of the system. The positions of the peaks match the corresponding positions of the acetone-glass interfaces measured by standard OCT. Notice that no peaks fall between the first and the second acetone peak in the molecularly-sensitive measurement. This indicates that CARS is in fact generated in both the first and second layers of acetone, and that the second peak is not simply due to the subsequent backscatter of the forward directed CARS from the first acetone layer. This result indicates that CARS can be generated over at least 600 μm of the depth-of-field of a low numerical aperture objective.

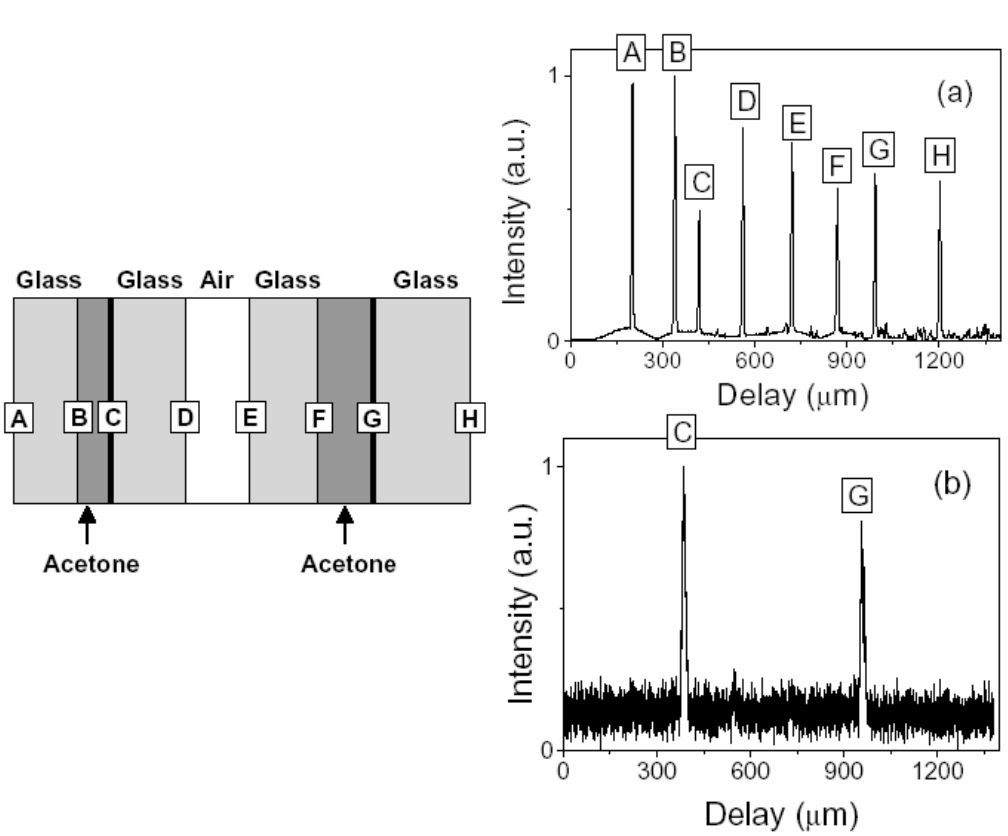

Figure 4: Coherent optical ranging. (a) OCT ranging and (b) CARS ranging through a sample stack.

3. INTERFEROMETRIC DIFFERENTIATION OF SIGNALS

A major impediment to the use of CARS to identify biological molecules is that the illumination levels required to produce a measurable signal often also produce a significantly larger nonresonant background signal from the medium. This is especially significant for water in biological tissues. The nonlinear interferometric techniques utilized in NIVI can also be used to differentiate which components of the measured signal are resonant and nonresonant. By using the interferometric time-gate to reject the early emitted nonresonant signal, we can identify the desired resonant component of the signal. This technique takes advantage of the persistence of intermediate states involved uniquely in the resonant process, and is applicable to most existing pulsed CARS illumination methods. This technique is demonstrated by examining the signals produced from acetone, which exhibits a resonance, and water, which does not.

Our approach is to utilize narrowband pump and Stokes pulses, but with the pump pulse stretched out in time to be approximately three times longer than the Stokes pulse. The shorter Stokes pulse coincides temporally with the leading edge of the pump pulse. A simulation was developed to illustrate this concept[38], with results presented in Figure 5. When the overlapped pump and Stokes pulses arrive, the molecule of interest is excited by stimulated Raman scattering. At the same time, a nonresonant four-wave-mixing signal is generated from the background. However, this nonresonant component ceases when the Stokes pulses passes. The molecule remains excited, though, and as the pump continues, the excitation is converted to anti-Stokes radiation by stimulated Raman scattering. The result is a resonant "tail" in the temporal interferogram as shown in Figure 5 (CARS/FWM interferogram). By delaying a reference pulse at the anti-Stokes frequency until after the nonresonant signal has passed, the reference acts as an interference gate to reject nonresonant components[38].

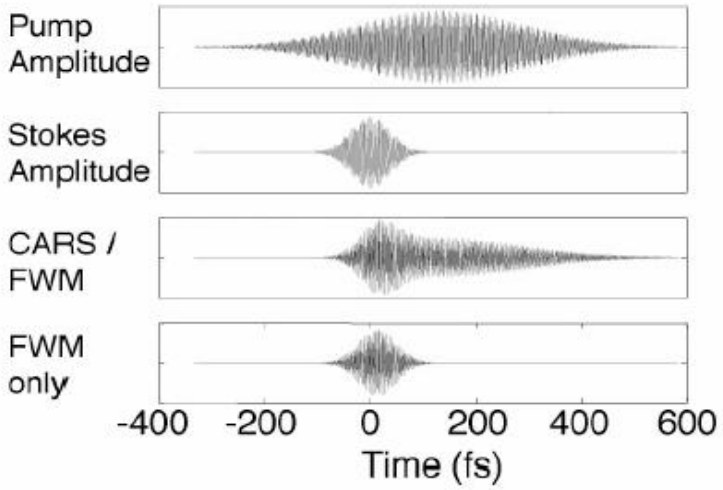

Figure 5: Simulation for differentiating resonant from nonresonant signals.

To demonstrate and validate this idea, we configured the experimental set-up shown in Figure 6 to measure the interferograms of anti-Stokes light produced by acetone and water. Acetone has a Raman resonance at 2925 cm^{-1} corresponding to the C-H stretch, while water does not, containing only hydrogen and oxygen. Water is of primary interest because it is a ubiquitous and pernicious source of non-resonant signal in

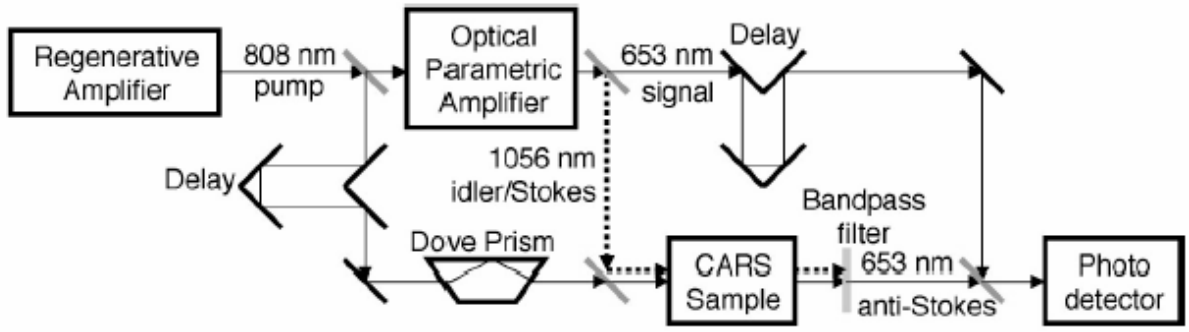

Figure 6: Experimental set-up for interferometrically differentiating resonant from nonresonant signals.

biological tissues. In the setup, a regenerative amplifier (RegA 9000, Coherent, Inc. Santa Clara, CA) emits pulses at 250 kHz repetition rate with 808 nm center wavelength and 20 nm bandwidth. These pulses are used both as the pump and also to seed a second-harmonic generation optical parametric amplifier (OPA) (OPA 9450, Coherent) which generates idler pulses with 1056 nm center wavelength and 20 nm bandwidth for use as a Stokes pulse. A 105 mm length BK7 glass Dove prism disperses the pump pulse to approximately three times the duration of the Stokes pulse. Note that there is a difference between the purpose of chirping the pulses here, and that of chirped CARS (c-CARS)[32]. Chirping here is done only to lengthen the pump pulse slightly so it only partially overlaps with the Stokes, while in c-CARS chirping serves to stretch the pulse to be essentially monochromatic over the lifetime of the resonance. The pump pulse is delayed to arrive at a dichroic beamsplitter at the same time as the Stokes pulse. The pulses are overlapped and are focused into the sample by a 30 mm focal length lens, which produces anti-Stokes radiation centered at 653 nm. The OPA signal is produced by two cascaded non-resonant three-wave-mixing steps that produce the same frequency as the four-wave-mixing process but with a far greater amount of power. Because the signal pulse is converted by non-resonant nonlinearities, and the OPA output is adjusted to maximize power, it is reasonable to expect the signal and idler are nearly transform-limited, and therefore will act as a brief time gate. The pump power at the sample was 20 mW, while the Stokes was 2 mW, with sufficient peak power to produce abundant resonant and non-resonant signals. At the same time, the signal pulse from the OPA, also at 653 nm, is used as the reference pulse. A Mach-Zehnder interferometer is used to combine the reference pulse and the CARS signal. The signals are attenuated by neutral density filters by many orders of magnitude before they are detected by a photomultiplier tube. By scanning the relative delay between the two signals, their interferometric cross-correlation was measured. Figure 7 shows the interferograms measured from acetone. The upper left plot shows the Raman spectrum of acetone near the probed resonance frequency. As can clearly be seen, the interferograms agree qualitatively with the simulation data in Figure 5. The acetone, having a persistent resonance, generates a resonant anti-Stokes “tail" with a length limited not by the lifetime of the resonance but by the length of the pump pulse, because the pump is needed to produce anti-Stokes radiation. As the pump/Stokes frequency difference is tuned away from the resonance at 2925 cm^{-1}, the resonant “tail" disappears. The tuning resolution is limited by the broad Stokes bandwidth of approximately 150 cm^{-1}, which is much wider than the Raman susceptibility linewidth.

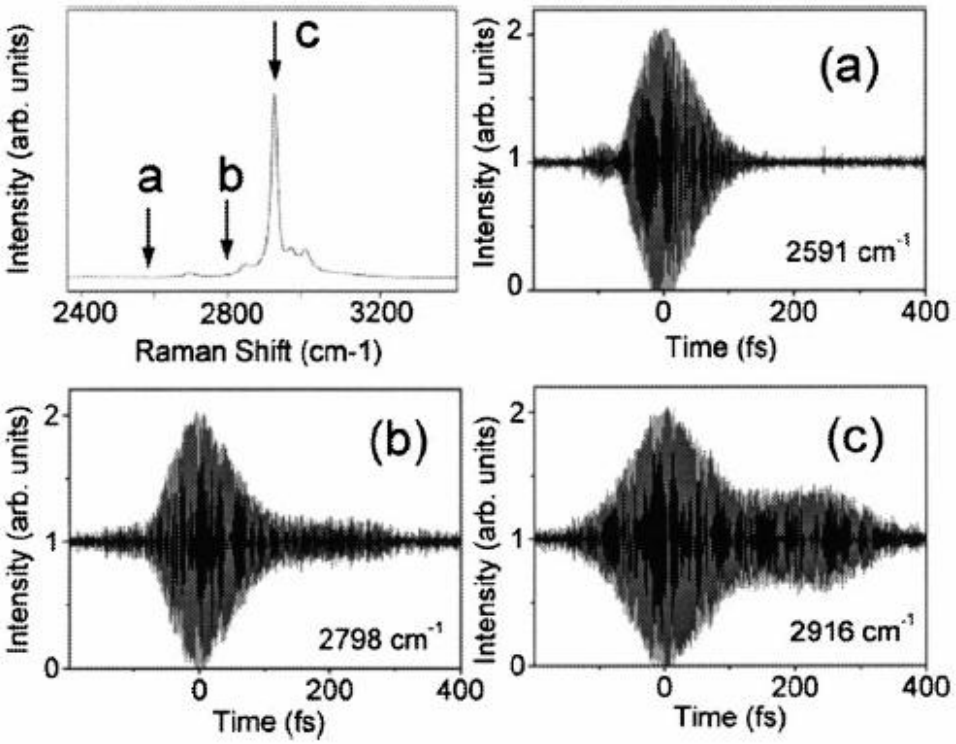

Figure 7: Cross-correlation interferograms of four-wave-mixing in acetone at various vibrational excitation frequencies (a-b). A portion of the Raman spectrum for acetone is shown (upper left), indicating the excitation frequencies where the interferograms were acquired.

To further test the ability to distinguish resonant and non-resonant materials, we filled a cuvette with acetone and water in various volumetric ratios. The concentration of acetone was inferred by observing the amount of power (total magnitude squared signal) in the resonant tail more than 120 fs after the non-resonant peak. Figure 8 shows the interferogram measured from water alone in the inset, which has no tail and is purely non-resonant. As the percentage of acetone is increased, the power of the anti-Stokes signal interference increases quadratically, exactly as expected, as shown in Figure 8. This demonstrates that the local oscillator remains stable enough to produce an accurate concentration measurement, whereas a nonresonant signal derived from the sample itself may fluctuate with material density and composition.

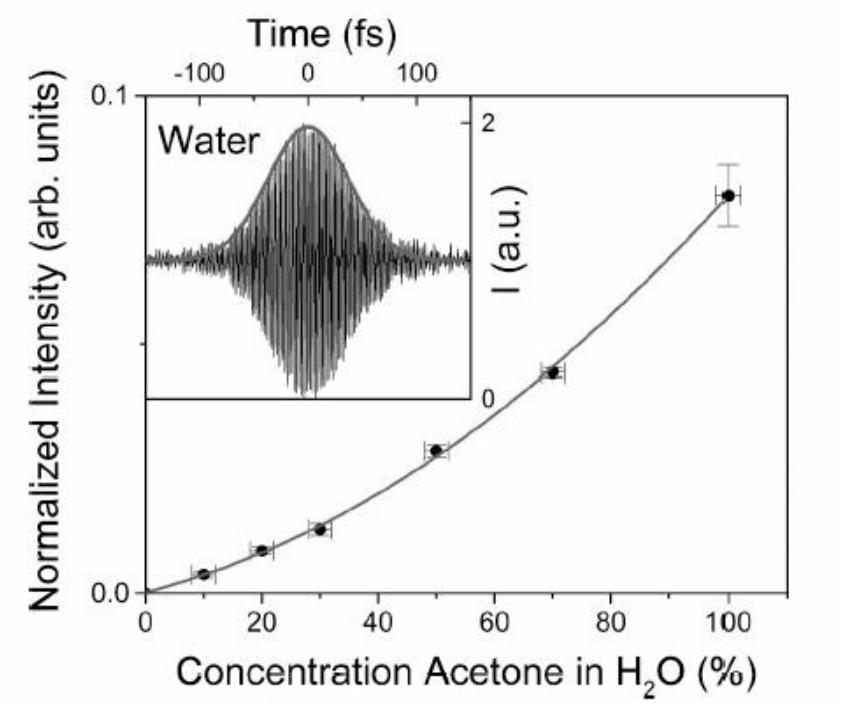

Figure 8: Interferogram from nonresonant four-wave-mixing in water (inset). The plot represents the power of the resonant anti-Stokes signal for various percentages of acetone in water by volume.

4. CONCLUSIONS

We have demonstrated a difference in the temporal evolution of anti-Stokes pulses produced by non-resonant and resonant four-wave-mixing processes. In this proof-of-principle experiment, the power utilized was large and the delay mechanism was too slow for practical scanning. We expect that data acquisition and imaging rates can be significantly increased by utilizing a rapidly dithered delay, or single-shot cross-correlation methods[39,40]. This approach utilizes nonlinear interferometry and appropriate reference and excitation pulses to measure the tail of resonant CARS. Such an approach will likely be very useful in CARS microscopy and NIVI[16,17] to eliminate the nonresonant background signal in addition to the other advantages that interferometric detection can provide, such as heterodyne sensitivity and stray light rejection.

In addition, we have also demonstrated coherent optical ranging of CARS which enables molecularly-sensitive optical ranging and OCT by combining the interferometric ranging technique used in OCT and the molecular identification capability of CARS. Depth-wise, cross-sectional imaging can be performed to demonstrate the unique molecular imaging capabilities of this technique. In the future, interferometric detection of CARS will not only provide advantages over traditional photon counting methods in CARS microscopy, but will also improve OCT image contrast of biological tissues by differentiating between tissue types based on molecular composition rather than linear elastic scattering.

ACKNOWLEDGMENTS

We thank Prof. P. Scott Carney for his helpful comments and acknowledge the scientific contributions and advice from Profs. Martin Gruebele, Dana Dlott, Amy Wiedemann, and Barbara Kitchell from the University of Illinois at Urbana-Champaign. This work was supported in part by the National Aeronautics and Space Administration (NAS2-02057, S.A.B.), the National Institutes of Health (National Cancer Institute), and the Beckman Institute for Advanced Science and Technology.

REFERENCES

1. D. Huang, E. A. Swanson, C. P. Lin, J. S. Schuman, W. G. Stinson, W. Chang, M. R. Hee, T. Flotte, K. Gregory, C. A. Puliafito, and J. G. Fujimoto, "Optical Coherence Tomography," Science 254(5035), pp. 1178-1181, 1991.
2. S. A. Boppart, G. J. Tearney, B. E. Bouma, J. F. Southern, M. E. Brezinski, and J. G. Fujimoto, "Noninvasive assessment of the developing *Xenopus* cardiovascular system using optical coherence tomography," Proc. Natl. Acad. Sci. USA 94, pp. 4256-4261, 1997.
3. S. A. Boppart, B. E. Bouma, C. Pitris, J. F. Southern, M. E. Brezinski, and J. G. Fujimoto, "*In vivo* cellular optical coherence tomography imaging," Nature Medicine 4, pp. 861-864, 1998.
4. J. G. Fujimoto, C. Pitris, S. A. Boppart, and M. E. Brezinski, "Optical coherence tomography: an emerging technology for biomedical imaging and optical biopsy," Neoplasia 2, pp. 9-25, 2000.
5. J. M. Schmitt, S. H. Xiang, and K. M. Yang, "Differential absorption imaging with optical coherence tomography," J. Opt. Soc. Am. A 15, pp. 2288-2296, 1998.
6. U. Morgner, W. Drexler, F. X. Kartner, X. D. Li, C. Pitris, E. P. Ippen, and J. G. Fujimoto, "Spectroscopic optical coherence tomography," Opt. Lett. 25, pp. 111-113, 2000.
7. R. Leitgeb, M. Wojtkowski, A. Kowalczyk, C. K. Hitzenberger, M. Sticker, and A. F. Fercher, "Spectral measurement of absorption by spectroscopic frequency-domain optical coherence tomography," Opt. Lett. 25, pp. 820-822, 2000.
8. G. J. Tearney, M. E. Brezinski, J. F. Southern, B. E. Bouma, M. R. Hee, and J. G. Fujimoto, "Determination of the refractive index of highly scattering human tissue by optical coherence tomography," Opt. Lett. 20, pp. 2258-2260, 1995.
9. A. M. Zysk, J. J. Reynolds, D. L. Marks, P. S. Carney, and S. A. Boppart, "Projected index computed tomography," Opt. Lett. 28, pp. 701-703, 2003.
10. J. F. de Boer, T. E. Milner, M. J. C. van Germert, and J. S. Nelson, "Two-dimensional birefringence imaging in biological tissue by polarization sensitive optical coherence tomography," Opt. Lett. 22, pp. 934-936, 1997.
11. C. K. Hitzenberger, E. Gotzinger, M. Sticker, M. Pircher, and A. F. Fercher, "Measurement and imaging of birefringence and optic axis orientation by phase resolved polarization sensitive optical coherence tomography," Opt. Express 9, pp. 780-790, 2001.
12. S. Jiao and L. V. Wang, "Two-dimensional depth-resolved Mueller matrix of biological tissue measured with double-beam polarization sensitive optical coherence tomography," Opt. Lett. 27, pp. 101-103, 2002.
13. B. H. Park, C. Saxer, S. M. Srinivas, J. S. Nelson, and J. F. de Boer, "*In vivo* burn depth determination by high-speed fiber-based polarization sensitive optical coherence tomography," J. Biomed. Opt. 6, pp. 474- 479, 2001.
14. T. M. Lee, A. L. Oldenburg, S. Sitafalwalla, D. L. Marks, W. Luo, F. J.-J. Toublan, K. S. Suslick and S. A. Boppart, "Engineered microsphere contrast agents for optical coherence tomography," Opt. Lett. **28,** 1546 (2003).
15. C. Yang, M. A. Choma, L. E. Lamb, J. D. Simon and J. A. Izatt, "Protein-based molecular contrast optical coherence tomography with phytochrome as the contrast agent," Opt. Lett. **29,** 1396 (2004).
16. D. L. Marks and S. A. Boppart, "Nonlinear interferometric vibrational imaging," Phys. Rev. Lett. 92(12), pp. 123905-1-123905-4, 2004.
17. C. Vinegoni, J. S. Bredfeldt, D. L. Marks, and S. A. Boppart, "Nonlinear optical contrast enhancement for optical coherence tomography," Opt. Express 12(2), pp. 331-341, 2004.
18. Y. Jiang, I. Tomov, Y. Wang and Z. Chen, "Second-harmonic optical coherence tomography," Opt. Lett. 29, pp. 1090-1092, 2004.
19. J.-X. Cheng and X. S. Xie, "Coherent anti-Stokes Raman scattering microscopy: Instrumentation, theory, and applications," J. Phys. Chem. B 108, 827-840, 2004.

20. Y. Yacoby, R. Fitzgibbon and B. Lax, "Coherent Cancellation of Background in Four-Wave Mixing Spectroscopy," J. Appl. Phys. 51**,** 3072-3077, 1980.
21. M. D. Duncan, J. Reintjes, and T. J. Manuccia, "Scanning coherent anti-Stokes Raman microscope," Opt. Lett. 7(8), pp. 350-352, 1982.
22. A. Zumbusch, G. R. Holtom, and X. S. Xie, "Three-dimensional vibrational imaging by coherent anti-Stokes Raman scattering," Phys. Rev. Lett. 82(20), pp. 4142-4145, 1999.
23. N. Dudovich, D. Oron, and Y. Silberberg, "Single-pulse coherent controlled nonlinear Raman spectroscopy and microscopy," Nature 418, pp. 512-514, 2002.
24. A. Volkmer, J.-X. Cheng, and X. S. Xie, "Vibrational imaging with high sensitivity via epidetected coherent anti-Stokes Raman scattering microscopy," Phys. Rev. Lett. 87(2), pp. 023901-1-023901-4, 2001.
25. E. O. Potma, D. J. Jones, J.-X. Cheng, X. S. Xie, and J. Ye, "High-sensitivity coherent anti-Stokes Raman scattering microscopy with two tightly synchronized picosecond lasers," Opt. Lett. 27, pp. 1168-1170, 2002.
26. J.-X. Cheng, Y. K. Jia, G. Zheng, and X. S. Xie, "Laser-scanning coherent anti-Stokes Raman scattering microscopy and applications of cell biology," Biophys. J. 83, pp. 502-509, 2002.
27. N. Dudovich, D. Oron, and Y. Silberberg, "Single-pulse coherent anti-Stokes Raman spectroscopy in the fingerprint spectral region," J. of Chem. Phys. 118(20), pp. 9208-9215, 2003.
28. J.-X. Cheng, A. Volkmer, L. D. Book, and X. S. Xie, "An epi-detected anti-Stokes Raman scattering (E-CARS) microscope with high spectral resolution and high sensitivity," J. of Phys. Chem. B 105, pp. 1277-1280, 2001.
29. M. Wojtkowski, A. Kowalczyk, R. Leitgeb, and A. F. Fercher, "Full range complex spectral optical coherence tomography technique in eye imaging," Opt. Lett. 27, pp. 1415-1417, 2002.
30. J. F. de Boer, B. Cense, B. H. Park, M. C. Pierce, G. J. Tearney, and B. E. Bouma, "Improved signal-to-noise ratio in spectral-domain compared with time-domain optical coherence tomography," Opt. Lett. 28, pp. 2067-2069, 2003.
31. E. Gershgoren, R. A. Bartels, J. T. Fourkas, R. Tobey, M. M. Murnane, and H. C. Kapteyn, "Simplified setup for high-resolution spectroscopy that uses ultrashort pulses," Opt. Lett. 28(5), pp. 361-363, 2003.
32. K. P. Knutsen, J. C. Johnson, A. E. Miller, P. B. Petersen, and R. J. Saykally, "High spectral resolution multiplex CARS microscopy using chirped pulses," Chem. Phys. Lett. 387, pp. 436-441, 2004.
33. A. M. Weiner, D. E. Leaird, G. P. Wiederrech, and K. A. Nelson, "Femtosecond pulse sequences used for optical manipulation of molecular motion," Science 247(4948), pp. 1317-1319, 1990.
34. D. Oron, N. Dudovich, D. Yelin, and Y. Silberberg, "Narrow-band coherent anti-Stokes Raman signals from broad-band pulses," Phys. Rev. Lett. 88(6), pp. 063004-1-063004-4, 2002.
35. D. Oron, N. Dudovich, D. Yelin, and Y. Silberberg, "Quantum control of coherent anti-Stokes Raman processes," Phys. Rev. A 65, pp. 043408-1-043408-4, 2002.
36. D. Oron, N. Dudovich, and Y. Silberberg, "Femtosecond phase-and-polarization control for background-free coherent anti-Stokes Raman spectroscopy," Phys. Rev. Lett. 90(21), pp. 213902-1-213902-4, 2002.
37. J. S. Bredfeldt, C. Vinegoni, D. L. Marks, and S. A. Boppart, "Molecularly-sensitive optical coherence tomography," Opt. Lett., In press, 2004.
38. D. L. Marks, C. Vinegoni, J. S. Bredfeldt, and S. A. Boppart, "Interferometric differentiation between resonant coherent anti-Stokes Raman scattering and nonresonant four-wave-mixing processes," Appl. Phys. Lett. 85, pp. 5787-5789, 2004.
39. K. G. Purchase, D. J. Brady, and K. Wagner, "Time-of-flight cross correlation on a detector array for ultrafast packet detection," Opt. Lett. 18, pp. 2129-2131, 1993.
40. L. Lepetit, G. Cheriaux, and M. Joffre, "Linear techniques of phase measurement by femtosecond spectral interferometry for applications in spectroscopy," J. Opt. Soc. Amer. B 12, pp. 2467-2474, 1995.